

Latest AMS results on the positron fraction and the \bar{p}/p ratio.

Andrei Kounine^{*†}

Massachusetts Institute of Technology, Cambridge, USA

E-mail: Andrei.Kounine@cern.ch

A precision measurement of the positron fraction in primary cosmic rays in the energy range from 0.5 to 500 GeV based on 10.9 million positron and electron events is presented. This measurement extends the energy range of our previous observation and increases its precision. The new results show that above ~ 200 GeV the positron fraction no longer exhibits an increase with energy. A measurement of the \bar{p}/p ratio in the rigidity range from 0.5 to 450 GV is also presented.

*The 34th International Cosmic Ray Conference,
30 July- 6 August, 2015
The Hague, The Netherlands*

*Speaker.

†on behalf of the AMS Collaboration

1. AMS Detector

The Alpha Magnetic Spectrometer, AMS-02, is a general purpose high energy particle physics detector. It was installed on the International Space Station, ISS, on 19 May 2011 to conduct a unique long duration mission (~ 20 years) of fundamental physics research in space. Reported results are based on the data collected during the first three years of operations on the ISS, corresponding to 41 billion of cosmic ray events for the positron fraction measurement and 54 billion events for the measurement of the \bar{p}/p ratio [1]. Due to the excellent and steady performance of the detector, the measurement of the positron fraction is extended up to 500 GeV with improved precision and the measurement of the \bar{p}/p ratio is extended to 450 GeV.

The layout of the AMS-02 detector [2] is shown in Figure 1. It consists of 9 planes of precision silicon Tracker; a Transition Radiation Detector, TRD; four planes of Time of Flight counters, TOF; a Magnet; an array of anti-coincidence counters, ACC, surrounding the inner Tracker; a Ring Imaging Čerenkov detector, RICH; and an Electromagnetic Calorimeter, ECAL. The figure also shows a high energy positron of 369 GeV recorded by AMS.

Three main detectors allow powerful separation between protons and electrons. These are the TRD, the ECAL and the Tracker. The TRD and the ECAL are separated by the Magnet and the Tracker. The matching of the ECAL energy and the momentum measured with the Tracker greatly improves the discrimination between protons and electrons.

The Tracker determines the trajectory and absolute charge (Z) of cosmic rays by multiple measurements of the coordinates and energy loss. Coordinate resolution of each plane is measured to be better than $10\ \mu\text{m}$ in the bending direction and the charge resolution is $\Delta Z \approx 0.06$ at $Z = 1$. Together with the Magnet, the Tracker provides a Maximum Detectable Rigidity of 2 TV [3].

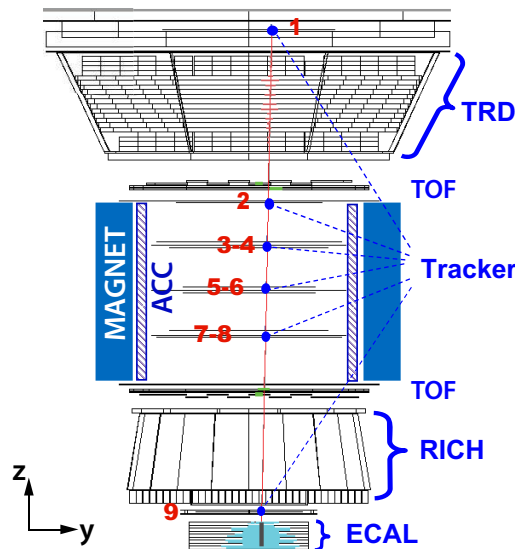


Figure 1: A 369 GeV positron event as measured by the AMS detector on the ISS in the (y - z) plane. Tracker planes 1-9 measure the particle charge, sign and momentum. The TRD identifies the particle as an electron/positron. The TOF measures the charge and ensures that the particle is downward-going. The RICH measures the charge and velocity. The ECAL independently identifies the particle as an electron/positron and measures its energy.

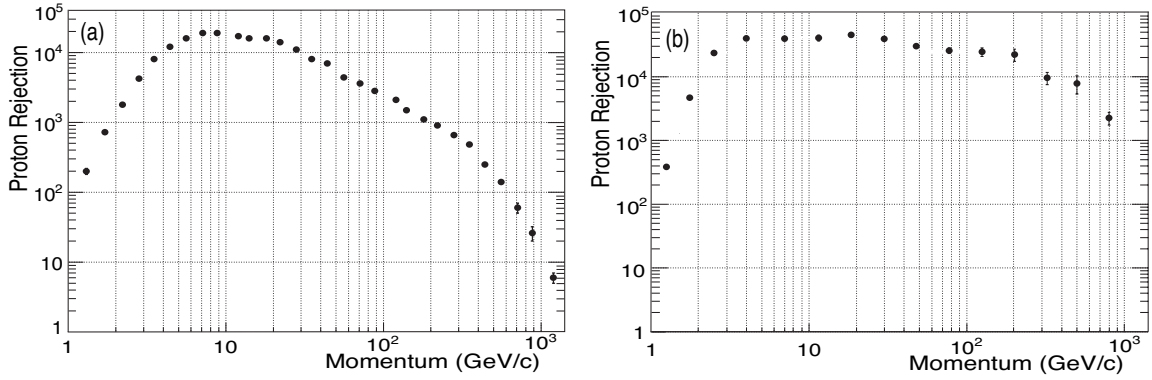


Figure 2: (a) The proton rejection measured by the TRD as a function of track momentum at 90 % selection efficiency for e^\pm . (b) The measured proton rejection using the ECAL and the Tracker. For 90 % e^\pm ECAL selection efficiency, the measured proton rejection is $\sim 10,000$ for the combination of the ECAL and the Tracker in the momentum range 3–500 GeV/c, independent of the TRD.

The TRD uses transition radiation to distinguish between e^\pm and protons, and dE/dx to independently identify nuclei [4]. It consists of 5,248 proportional tubes of 6 mm diameter arranged in 20 layers interleaved with a 20 mm thick fiber fleece radiator. To differentiate between e^\pm and protons, signals from the 20 layers are combined in a TRD estimator formed from the ratio of the log-likelihood probability of the e^\pm hypothesis to that of the proton hypothesis. The proton rejection power of the estimator at 90 % e^\pm efficiency measured up to 10^4 , as shown in Figure 2a.

The ECAL consists of a multilayer sandwich of 98 lead foils and $\sim 50,000$ scintillating fibers with an active area of $648 \times 648 \text{ mm}^2$ and a thickness of 166.5 mm corresponding to 17 radiation lengths [5]. The calorimeter is composed of 9 superlayers, with the fibers running in one direction only in each superlayer. The 3-D imaging capability of the detector is obtained by stacking alternate superlayers with fibers parallel to the x- and y-axes (5 and 4 superlayers, respectively). The energy resolution of the ECAL is $\sigma(E)/E = \sqrt{(0.104)^2/E + (0.014)^2}$. To cleanly separate protons from electrons and positrons, an ECAL estimator, based on a Boosted Decision Tree, BDT, algorithm [6], is constructed using the 3-D shower shape in the ECAL. The proton rejection power of the ECAL estimator when combined with the energy-momentum matching requirement $E/p > 0.75$ reaches $\sim 10,000$ (see Figure 2b), as determined from the ISS data.

Monte Carlo simulated events are produced using a dedicated program developed by AMS which is based on the GEANT-4.9.4 package [7]. This program simulates electromagnetic and hadronic interactions of particles in the materials of AMS and generates detector responses. The digitization of the signals, including those of the AMS trigger, is simulated precisely according to the measured characteristics of the electronics. The digitized signals then undergo the same reconstruction as used for the data. The Monte Carlo samples used in the present analysis have sufficient statistics so they do not contribute to the errors.

2. Positron fraction measurement.

Electron and positron events are selected by requiring a track in the TRD and in the Tracker, a cluster of hits in the ECAL and a measured velocity $\beta \sim 1$ in the TOF consistent with a downward-going $Z = 1$ particle. In order to reject $> 99\%$ of the remaining protons, an energy-dependent cut on

the ECAL estimator is applied. In order to reject positrons and electrons produced by the interaction of primary cosmic rays with the atmosphere [8], the energy measured with the ECAL is required to exceed by a factor of 1.2 the maximal Stoermer cutoff [9] for either a positive or a negative particle at the geomagnetic location where the particle was detected at any angle within the AMS acceptance. The resulting acceptance for electrons and positrons is identical and nearly constant over the range from 3 to 500 GeV. It takes into account the geometric acceptance, the selection efficiency, and the trigger efficiency. The integrated acceptance for positrons and electrons is the same within our statistics and cancels in the fraction.

The positron fraction is determined in ECAL energy bins. The binning is chosen according to the energy resolution and the available statistics such that migration of the signal events to neighboring bins has a negligible contribution to the systematic errors above ~ 2 GeV. The energy scale is verified by using minimum ionizing particles and the ratio E/p . In each energy bin, the 2-dimensional reference spectra for e^\pm and the background are fit to data in the [TRD estimator- $\log(E/p)$] plane by varying the normalizations of the signal and the background. The reference spectra are determined from high statistics electron and proton data samples selected using tracker and ECAL information including charge sign, track-shower axis matching, and the ECAL estimator. The fit is performed simultaneously for the positive and negative rigidity data samples in each energy bin yielding the number of positrons, the number of electrons, the number of protons, and the amount of charge confusion, which is defined as the fraction of electrons or positrons reconstructed with a wrong charge sign. From the bin-by-bin fits, the sample contains 10.3×10^6 electrons, 0.64×10^6 positrons and 3.50×10^6 protons. To evaluate the systematic uncertainty related to event selection, the complete analysis is repeated in every energy bin over 1000 times with different cut values, such that the selection efficiency varies up to 30%. The distribution of the positron fraction resulting from these 1000 analyses contains both statistical and systematic effects. The difference between the width of this distribution from data and from Monte Carlo simulation quantifies this systematic uncertainty. Systematic effects due to the charge confusion were stud-

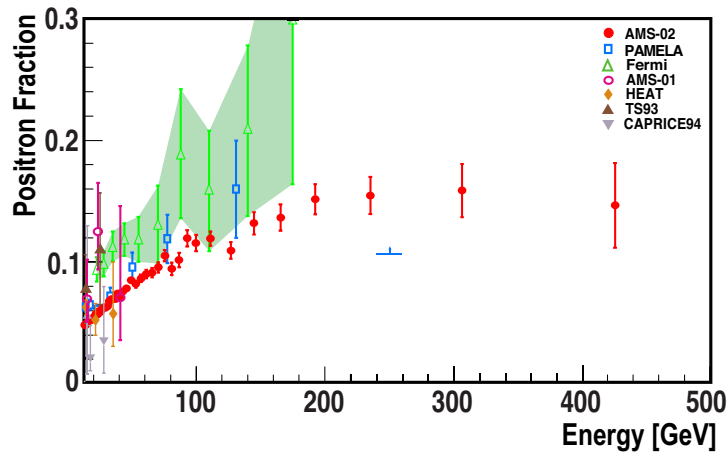


Figure 3: The positron fraction above 10 GeV, where it begins to increase. The present measurement extends the energy range to 500 GeV and demonstrates that above ~ 200 GeV the positron fraction is no longer increasing. Measurements from PAMELA [14] (the horizontal blue line is their lower limit), Fermi-LAT [15], and other experiments [10, 11, 12, 13] are also shown.

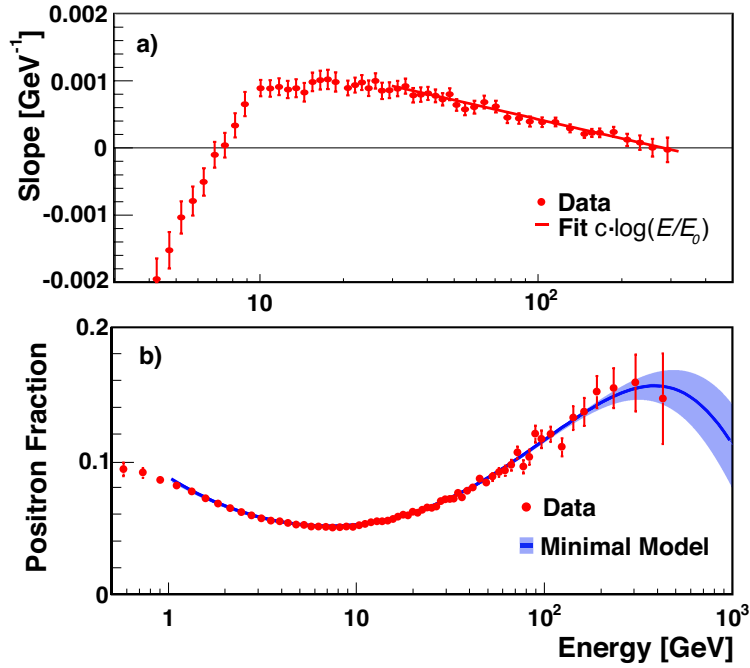


Figure 4: (a) The slope of the positron fraction vs. energy over the entire energy range (the values of the slope below 4 GeV are off scale). The line is a logarithmic fit to the data above 30 GeV. (b) The positron fraction measured by AMS and the fit of a minimal model (solid curve, see text) and the 68% C.L. range of the fit parameters (shaded). The error bars are the quadratic sum of the statistical and systematic uncertainties.

ied using control data samples of electron events where the ionization in the lower TOF counters corresponds to at least two traversing particles. The systematic errors are obtained by varying the background normalizations within the statistical limits and comparing the results with the Monte Carlo simulation. The systematic error associated with the uncertainty of the data derived reference spectra arises from their finite statistics. It is measured by varying the shape of the reference spectra within the statistical uncertainties. Its contribution to the overall error is small compared to the statistical uncertainty of data and is included in the total systematic error.

The measured positron fraction is presented in Figure 3 as a function of the reconstructed energy at the top of the AMS detector. The increase of the positron fraction has been reported by earlier experiments: TS93 [10], Wizard/CAPRICE [11], HEAT [12], AMS-01 [13], PAMELA [14] and Fermi-LAT [15]. The new result extends the energy range to 500 GeV and is based on a significant increase in the statistics. Fig. 3 explores the behavior of the positron fraction at high energies (>10 GeV) and compares it with earlier measurements. We observe that above ~ 200 GeV the positron fraction is no longer increasing with energy.

To examine the energy dependence of the positron fraction quantitatively in a model independent way, straight line fits were performed over the entire energy range with a sliding energy window, where the width of the window varies with energy to have sufficient sensitivity to the slope. The variation of the slope of the positron fraction from 4 GeV upwards is shown in Fig. 4a. As seen in the figure, above 30 GeV the slope decreases logarithmically with energy. Fitting the change of the slope as a function of energy above 30 GeV with a 2 parameter fit ($\text{slope} = c \cdot \log(E/E_0)$) where c is the normalization and E_0 is the energy at which the slope crosses zero, that is, the energy at

which the positron fraction reaches its maximum) results in a determination of $E_0 = 275 \pm 32$ GeV with a $\chi^2/d.f. = 3.9/12$ taking into account correlations. The result of the fit is shown as a solid line in Fig. 4a. Figure 4b shows the measure positron fraction together with a minimal model [1] fit (a solid curve together with the 68% C.L. range of the fit parameters). The fit in the energy range from 1 to 500 GeV yields a $\chi^2/d.f. = 36.4/58$, leading to the conclusion that no fine structures are observed in the data.

Following the publication of our papers [1], there have been many interpretations [16] with two popular classes. In the first, the excess of e^+ comes from pulsars. In this case, after flattening out with energy the positron fraction will begin to slowly decrease and a dipole anisotropy should be observed. In the second, the shape of the positron fraction is due to dark matter collisions. In this case, after flattening out, the fraction will decrease rapidly with energy due to the finite and specific mass of the dark matter particle and no dipole anisotropy will be observed. Over its lifetime, AMS will reach a dipole anisotropy sensitivity of $\delta \simeq 0.01$ at the 95% C.L.

3. Measurement of the \bar{p}/p ratio.

Proton and antiproton cosmic ray events are selected by requiring a track in the TRD and in the Tracker, a cluster of hits in the ECAL and a measured velocity $\beta > 0.3$ in the TOF consistent with a downward-going $Z = 1$ particle. In order to reject remaining electrons and positrons, an energy-dependent cut on the ECAL estimator is applied. In order to reject particles produced by the interaction of primary cosmic rays with the atmosphere [8], the rigidity measured in the tracker is required to exceed by a factor of 1.2 the maximal Stoenmer cutoff [9] for either a positive or a negative particle at the geomagnetic location where the particle was detected at any angle within the AMS acceptance.

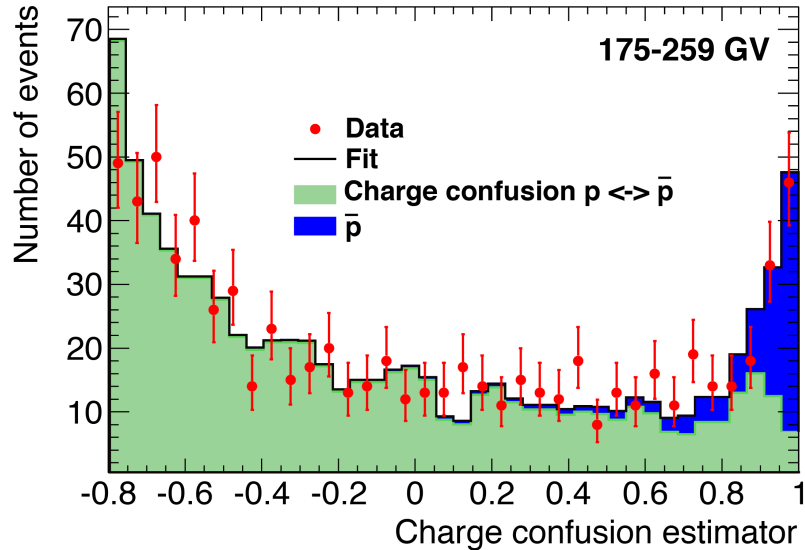


Figure 5: Spectrum of the charge confusion estimator for the negative rigidity bin 175–259 GV (red dots). Fit of the two reference spectra (the antiproton signal - dark shade, and the background from the charge confusion protons - light shade) to date are also shown.

The resulting acceptance for protons and antiprotons is calculated taking into account the geometrical acceptance, the selection efficiency, and the trigger efficiency and the inelastic cross-sections for protons and antiprotons that have different rigidity dependence in the range from 0.5 to 1000 GV. The ratio \bar{p}/p is then determined in tracker energy bins. The binning is chosen according to the energy resolution and the available statistics such that migration of the signal events to neighboring bins has a negligible contribution to the systematic errors. At this stage of the analysis the positive rigidity sample contains only protons, whereas the negative rigidity sample comprises both antiprotons (signal) and protons with the negative charge wrongly identified in the tracker (background). To separate these two classes of the events in the negative rigidity sample a charge confusion estimator is constructed based on a BDT algorithm [6] that uses 10 variables from the tracker and the TOF. In each rigidity bin, the reference spectra of the charge confusion estimator for the signal and the background are fit to data by varying the normalizations of the signal and the background. The signal reference spectra are determined from high statistics proton data sample, whereas the background spectrum is determined from the Monte Carlo simulation. The fit is performed each rigidity bin yielding the number of antiprotons and the amount of charge confusion background. Example of the fit is presented in Figure 5 for the rigidity bin 175–259 GV. From the bin-by-bin fits, the selected sample contains a total 2.9×10^5 of antiprotons.

There are several systematic uncertainties. However, at high rigidities the accuracy of the measurement is still limited by statistics. For instance, in the rigidity bin 175–259 GV statistical error from the fit amounts to 14.4% of the measured value, whereas total systematic uncertainty is only 7.3% with the following breakdown: the acceptance uncertainty and bin-to-bin migration – 1.4%; the selection uncertainty – 2.1%; and the uncertainty in the reference spectra – 6.9%.

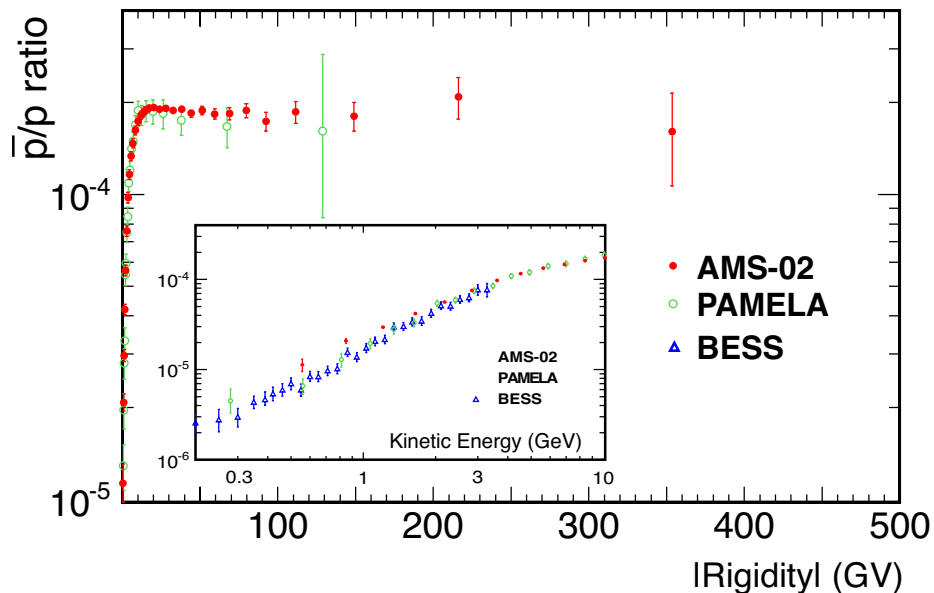


Figure 6: The AMS results on the ratio \bar{p}/p . The present measurement extends the energy range to 450 GeV and demonstrates that above ~ 100 GeV the \bar{p}/p remains almost flat. Measurements from BESS [17] and PAMELA [18] are also shown.

The measured ratio \bar{p}/p is presented in Figure 6 as a function of rigidity at the top of the AMS detector. Results reported by the earlier experiments: BESS [17] and PAMELA [18] are also shown. The new AMS results extend the rigidity range to 450 GV and increase precision of the measurement. It shows that above $\sim 100\text{GeV}$ the \bar{p}/p remains almost flat with rigidity.

References

- [1] M. Aguilar *et al.*, Phys. Rev. Lett. **A 110** (2013) 141102;
L. Accardo *et al.*, Phys. Rev. Lett. **A 113** (2014) 141102;
A. Kounine, presentation at “AMS Days at CERN”, CERN, 15 April 2015.
- [2] A. Kounine, Int. J. Mod. Phys. **E 21** (2012) 123005.
- [3] B. Alpat *et al.*, Nucl. Instrum. Meth. **A 613** (2010) 207.
- [4] Th. Kirn, Nucl. Instrum. Meth. **A 706** (2013) 43;
P. Doetinchem *et al.*, Nucl. Instrum. Meth. **A 558** (2006) 526;
F. Hauler *et al.*, IEEE Trans. Nucl. Sci. **51** (2004) 1365.
- [5] C. Adloff *et al.*, Nucl. Instrum. Meth. **A 714** (2013) 147.
- [6] B. Roe *et al.*, Nucl. Instrum. Meth. **A 543** (2005) 577.
- [7] J. Allison *et al.*, IEEE Trans. Nucl. Sci. **53** (2006) 270; S. Agostinelli *et al.*, Nucl. Instrum. Meth. **A 506** (2003) 250.
- [8] J. Alcaraz *et al.*, Phys. Lett. **B 484** (2000) 10.
- [9] C. Stoermer, The Polar Aurora, Oxford University Press, London (1950).
- [10] R. Golden *et al.*, Astrophys. J. **457** (1996) L103.
- [11] M. Boezio *et al.*, Adv. Sp. Res. **27-4** (2001) 669.
- [12] J. J. Beatty *et al.*, Phys. Rev. Lett. **93** (2004) 241102; M. A. DuVernois *et al.*, Astrophys. J. **559** (2001) 296.
- [13] M. Aguilar *et al.*, Phys. Lett. **B 646** (2007) 145.
- [14] O. Adriani *et al.*, Phys. Rev. Lett. **111** (2013) 081102;
O. Adriani *et al.*, Astropart. Phys. **34** (2010) 1;
O. Adriani *et al.*, Nature **458** (2009) 607.
- [15] M. Ackermann *et al.*, Phys. Rev. Lett. **108** (2012) 011103.
- [16] There are many recent excellent theoretical articles on the positron fraction. A few examples are:
L. Feng *et al.*, Phys. Lett. **B 728** (2014) 250;
K. Blum *et al.*, Phys. Rev. Lett. **111** (2013) 211101;
L. Bergström *et al.*, Phys. Rev. Lett. **111** (2013) 171101;
J. Kopp, Phys. Rev. **D 88** (2013) 076013;
I. Cholis and D. Hooper, Phys. Rev. **D 88** (2013) 023013;
T. Linden and S. Profumo, Astrophys. J. **772** (2013) 18.
- [17] K. Abe *et al.*, Phys. Rev. **B 670** (2008) 103.
- [18] O. Adriani *et al.*, Phys. Rev. Lett. **102** (2009) 051101.